

Occlusion-aware Risk Assessment and Driving Strategy for Autonomous Vehicles Using Simplified Reachability Quantification

Hyunwoo Park¹, Jongseo Choi¹, Hyuntai Chin¹, Sang-Hyun Lee² and Doosan Baek^{1,2*}

Abstract—One of the unresolved challenges for autonomous vehicles is safe navigation among occluded pedestrians and vehicles. Previous approaches included generating phantom vehicles and assessing their risk, but they often made the ego vehicle overly conservative or could not conduct a real-time risk assessment in heavily occluded situations. We propose an efficient occlusion-aware risk assessment method using *simplified reachability quantification* that quantifies the reachability of phantom agents with a simple distribution model on phantom agents' state. Furthermore, we propose a driving strategy for safe and efficient navigation in occluded areas that sets the speed limit of an autonomous vehicle using the risk of phantom agents. Simulations were conducted to evaluate the performance of the proposed method in various occlusion scenarios involving other vehicles and obstacles. Compared with the baseline case of no occlusion-aware risk assessment, the proposed method increased the traversal time of an intersection by 1.48 times but decreased the average collision rate and discomfort score by up to 6.14 times and 5.03 times, respectively. The proposed method has shown the state-of-the-art level of time efficiency with constant time complexity and computational time of less than 5 ms.

Index Terms—Collision Avoidance, Motion and Path Planning

I. INTRODUCTION

AUTONOMOUS vehicles and other mobile robots often use LiDAR, cameras, and radar to perceive their surroundings. However, these sensors generally only work according to the line-of-sight, which gives them a critical disadvantage in common occluded situations as shown in Fig. 1. A scenario with occluded areas can lead to potentially dangerous scenarios where other vehicles or pedestrians may suddenly appear in the route of the autonomous vehicle [1], [2]. Human drivers handle occlusion by decreasing velocity sufficiently to lower the risk without losing efficiency. For autonomous vehicles, a common approach to occlusion-aware risk assessment has been to generate phantom agents (PAs) in

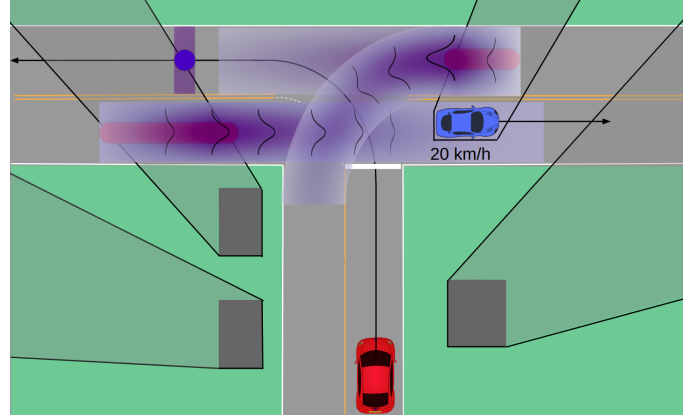


Fig. 1: Ego vehicle (red) entering an intersection. Occlusions due to obstacles (dark gray) and another vehicle (blue) are shaded in gray. Positions of potential hidden vehicles that can collide with the ego vehicle are indicated by red lines and blue point. The blue point has same direction with the ego vehicle, while the red lines do not. The risk along the centerline of the road due to potential hidden vehicles is represented as purple. The darker the purple gets, the riskier it is. Furthermore, the risk is proportional to a normal distribution where the random variable is the distance from the centerline of the road.

occluded areas. In [3], they proposed a set-based prediction method that considers every possible future behavior of PAs. However, they did not quantify the occlusion risk, which can make the ego vehicle behave overly conservatively. In [4], and [5], they quantified the occlusion risk by sampling particles that represent PAs in the occluded area. However, such an approach can lead to intensive computation in heavily occluded areas and make the risk assessment impossible to perform in real-time.

In this paper, we propose an efficient method for occlusion-aware risk assessment and a planning strategy for safe navigation through occluded areas. The risk assessment is based on *simplified reachability quantification* (SRQ) that quantifies the ability of the PAs to reach a certain position using a simple distribution model on the PAs' state. The model-based quantification derived constant time complexity of the proposed method. The planning strategy sets speed limit in a position where occlusion risk is presented. This strategy is effective and can be easily integrated with any other planning and control algorithms because it plans a safe motion of the ego vehicle using only speed limit.

The main contributions are as follows:

- The proposed method achieves constant time complexity and assesses heavily occluded scenarios in real time using SRQ.

Manuscript received: JULY, 31, 2023; Accepted OCTOBER, 13, 2023.

This paper was recommended for publication by Editor Aniket Bera upon evaluation of the Associate Editor and Reviewers' comments.

*This work was supported by the Korea Agency for Infrastructure Technology Advancement (KAIA) grant funded by the Ministry of Land, Infrastructure and Transport (RS-2021-KA160853, Road traffic Infrastructure monitoring and emergency recovery support service technology development).

¹ ThorDrive, Seoul, 07268, Republic of Korea

{hwpark, jschoi, htchin, dsbaek}@thordrive.ai

² Seoul National University, Seoul, Republic of Korea

slee01@snu.ac.kr

* Corresponding author

Digital Object Identifier (DOI): see top of this page.

- The proposed method can handle various types of driving environment, such as occluded vehicles in an intersection and occluded pedestrians behind street parking cars.
- The proposed method achieves remarkable decreases in ride discomfort and the collision rate compared to the baseline case of no occlusion-aware risk assessment.
- The proposed method is easily integrated with any other planning and control algorithms.

The remainder of the paper is organized as follows: Section II reviews related works of occlusion risk assessment and driving strategy utilizing it. Section III defines problem setting and primary concepts, which would be used in later sections. Section IV describes how our method finds PAs that are relevant to the ego vehicle and assesses their risks. Then, motion planning using the occlusion-aware risk assessment is proposed. Section V shows how our method is evaluated in the CARLA simulator [6] and the real world. Section VI analyzes the evaluation results and shows how the key metrics are improved. Section VII concludes the proposed method and discusses future works.

II. RELATED WORK

Previous approaches to occlusion-aware risk assessment can be divided into two categories, namely *probabilistic based methods* [4], [5], [7]–[9] and *over-approximation methods* [3], [10], [11]. There are also other methods variated from two methods and used concepts, such as *Sequential Reasoning* [11], [12]. These categories are briefly reviewed here.

Probabilistic methods quantify the occlusion risk by formulating the problem probabilistically. In [5], they sampled potential positions of the hidden *potential vehicles* (phantom vehicles) to assess the risk. However, they did not consider the types of the phantom vehicles to filter out unnecessary ones, and sampling the particles (phantom vehicles) was inefficient. In [4], they calculated backward reachability set (BRS) of every particle of forward reachability set (FRS) of the ego vehicle to assess the occlusion risk. This method can be inefficient particularly with a large number of particles in heavily occluded areas. In addition, they considered every possible control input of the phantom vehicles, which is computationally inefficient because most vehicles have few options when driving in the real world.

Over-approximation methods are a special case of probabilistic method [5] that consider the probability of every phantom vehicle as 100%. In [3], they used an *edge*, first introduced by [10], to classify *static* and *dynamic* phantom vehicles. The classification results were then used to assess the occlusion risk. Over-approximation methods are efficient because they don't quantify the risk, however they tend to make the ego vehicle behave conservatively and even freeze in some corner cases where the ego vehicle must take a risk to pass through.

Studies that used *sequential reasoning* considered only necessary agents based on observations over time. In [11], they used an *over-approximation method* to track hidden agents conservatively over time and formulate a passive safety (*p-safe*)

[13] planning strategy using *braking inevitable collision states* [14] and *responsibility sensitive safety* [15]. However, they tracked every possible agent within their sensor range, which is inefficient for heavily occluded areas and with long-range sensors.

Driving strategies differ depending on the approach used for occlusion-aware risk assessment. Among probabilistic methods, [5] used optimization to generate a trajectory with a low occlusion risk, [9] used a minimum cost function including an occlusion risk cost to select a trajectory, and [7] reduced the velocity of the ego vehicle when the risk was sufficiently high before it entered an intersection. Among over-approximation methods, [3], [10] obtained fail-safe trajectory [16], [17] that did not collide with any other phantom vehicles.

III. PRELIMINARIES

In this section, problem setting and primary concepts used in later sections will be defined. Let $t \in \mathbb{R}$ be the time, $x(t)$ be the state of the system at time t in the state space \mathcal{X} , and u be the ego vehicle's control input in the action space \mathbb{U} . The environment surrounding the ego vehicle comprises $n \in \mathbb{Z}$ number of lanes $l \in L$. Each lane l has a set of *continuous* and *sequential* centerline points denoted by P^l . The k -th lane l_k , where $(0 \leq k \leq n, k \in \mathbb{Z})$, has m centerline points $P^{l_k} = \{p_1^{l_k}, p_2^{l_k}, p_3^{l_k}, \dots, p_m^{l_k}\}$ in the Cartesian space $p \in P \subset \mathbb{R}^2$ and road width of l_w^k . The route of the ego vehicle is predefined as points following certain lanes $l \in L$ to reach the goal in the Cartesian space, which is represented as $route(x(t_0)) = \{x(t_0), x(t_1), x(t_2), \dots, x(t_k)\}$ where $x(t) \in \mathcal{X}$.

Definition 1. (Observable Polygon, \mathbb{O}). \mathbb{O} is generated by the line-of-sight sensors from the ego vehicle and comprises points p in the Cartesian space $p \in \mathbb{O} \subset \mathbb{R}^2$.

Definition 2. (Phantom Agent, PA). PA is a potential hidden agent outside the observable polygon and is modeled as a point mass that allows small agents like cyclists and children could be included. PAs can be further classified as phantom vehicles (PVs) or phantom pedestrians (PPs).

PVs are assumed to always be on the road and drive along the lane. They can have various velocities and even exceed the speed limit of the road. In contrast, PPs can be anywhere because they are not physically constrained unlike cars on the sidewalk. In [11], they also considered *illegally-behaving pedestrians* that walk on roads.

Definition 3. (Forward Reachable Set, FRS) Assume the vehicle's dynamics are described as following ordinary differential equation:

$$\dot{x}(t) = f(x(t), u(t)) \quad (1)$$

The FRS is a set of states that could be reached in given an initial state x_0 at time t_0 and fixed time horizon T_{fix} :

$$FRS(x_0, T_{\text{fix}}) := \{x(t) \in \mathcal{X} | \dot{x}(t) = f(x(t), u(t)), \forall u(t) \in \mathbb{U}, \forall t \in [t_0, t_0 + T_{\text{fix}}]\} \quad (2)$$

Definition 4. (Backward Reachable Set, BRS)

The BRS is a set of initial states x_0 at time t_0 that can reach the given final state x_f within the fixed time horizon T_{fix} :

$$BRS(x_f, T_{\text{fix}}) := \{x_0 \in \mathcal{X} \mid x_f \in FRS(x_0, T_{\text{fix}}), \forall u(t) \in \mathbb{U}, \dot{x}(t) = f(x(t), u(t)), \forall t \in [t_0, t_0 + T_{\text{fix}}]\} \quad (3)$$

IV. METHOD

The proposed method has three steps. First, PAs in occluded areas are generated by *node classification* (Section IV-A) and *inferring the phantom agent zone* (Section IV-B). Then, an approach we call *Simplified Reachability Quantification* (Section IV-C) that quantifies the reachability of the PVs is proposed. Next, the occlusion risks of PAs are defined by SRQ. Finally, a driving strategy that sets a speed limit depending on the occlusion risk is developed.

A. Node Classification

Node classification is based on the edge classification which classifies edges into static, dynamic, relevant, and irrelevant edges [3]. They over-approximate the shape of the PVs and represented PVs as edges. Static edges are PVs that have same direction with the ego vehicle, whereas dynamic edges are PVs in different direction than that of the ego vehicle. Relevant edges are PVs that can reach the route of the ego vehicle in the prediction horizon T_{pred} , while irrelevant edges are PVs that cannot reach the route of the ego vehicle. In [3], they also over-approximate the PVs' positions to be the closest position to the ego vehicle. In our method, node is introduced instead of the edge to obtain PV intervals and to avoid the over-approximations of the PVs.

Node classification is a sequence of procedures used to improve the efficiency of the risk assessment by classifying PVs according to whether they pose a *static* or *dynamic* risk to the ego vehicle and by removing irrelevant PVs. Figs. 2a-c show the three main steps of node classification.

1) *Intersection of Observable Polygon and Lanes*: *Intersecting nodes* \mathbb{I} are defined as the intersection of the observable polygon \mathbb{O} and the centerline of lanes P^{l_k} .

$$\mathbb{I} = \{p \in \mathbb{R}^2 \mid p = \mathbb{O} \cap P^{l_k}, k \in \{1, 2, 3, \dots, m\}\} \quad (4)$$

\mathbb{I} are used to find the potential positions of PVs. \mathbb{I} that overlap with or are too close to other vehicles that even small agents cannot exist are excluded.

2) *Static/Dynamic Node Classification*: The intersecting nodes \mathbb{I} are then classified as static nodes \mathbb{S} or dynamic nodes \mathbb{D} . \mathbb{I} are classified as \mathbb{S} if it has any intersection with $FRS(x_{ego}, T_{\text{pred}})$, and the remainder of \mathbb{I} are classified as \mathbb{D} :

$$\mathbb{S} = FRS(x_{ego}, T_{\text{pred}}) \cap \mathbb{I}, \quad \mathbb{D} = \mathbb{I} - \mathbb{S} \quad (5)$$

\mathbb{S} can be visited by the ego vehicle in the given time horizon, but \mathbb{D} cannot. Note that the concept of static and dynamic are used to characterize other terms in the following sections.

3) *Relevant/Irrelevant Node Classification*: Next, the static nodes \mathbb{S} and dynamic nodes \mathbb{D} need to be classified as *relevant* or *irrelevant* nodes. Irrelevant nodes do not need to be considered because their FRS does not collide with the route of the ego vehicle within T_{pred} . A node is classified as *relevant* (\mathbb{RN}) if $FRS(i, T_{\text{pred}})$, where $i \in \mathbb{I}$, collides with the route of the ego vehicle and as *irrelevant* (\mathbb{IN}) if it does not:

$$\begin{aligned} \mathbb{RN} &= \{i \in \mathbb{I} \mid FRS(i, T_{\text{pred}}) \cap \text{route}(x(t_0)) \neq \emptyset\} \\ \mathbb{IN} &= \{i \in \mathbb{I} \mid FRS(i, T_{\text{pred}}) \cap \text{route}(x(t_0)) = \emptyset\} \end{aligned} \quad (6)$$

However, if $i \in \mathbb{S}$, then only the first \mathbb{S} reached by the route of the ego vehicle is considered relevant [3] because the risk of the other \mathbb{S} is accounted for by the first one. Note that the concept of relevance is used to characterize other terms in the following sections.

B. Inferring the phantom agent zone

The *phantom agent zone* is a set of occluded points where *relevant* PAs exist. It comprises the *phantom vehicle zone* (PVZ) and *phantom pedestrian zone* (PPZ). The PVZ comprises the *phantom vehicle set* (PVS), which is a set of occluded points in a lane that are continuously connected to each other. We assume that one *relevant* PV exists in every PVS, therefore every PVS must include at least one *relevant node* \mathbb{RN} . If a PVS includes a *relevant* \mathbb{D} , it is defined as a *dynamic* PVS. However, if it includes *relevant* \mathbb{S} , then only the *relevant* \mathbb{S} is defined as the *static* PVS. In Fig. 2d, the dynamic PVS is represented as a red line, while the static PVS is represented as blue dot.

1) *Static Phantom Vehicle Set*: Defining the static PVS as encompassing the positions of every PV that poses a static risk to the ego vehicle is dangerous and inefficient because the occlusion risk would be scattered. Furthermore, we have observed that the static occlusion risk is often removed before it affects the ego vehicle. Therefore, the most efficient and safest way to consider the positions of static PVs is to define the static PVS as encompassing the positions of relevant \mathbb{S} .

2) *Dynamic Phantom Vehicle Set*: The dynamic PVS is obtained as follows. First, the dynamic relevant nodes are taken as the starting point of the dynamic PVS. Then, new points p_{new} are added to the dynamic PVS in the reverse direction of the lane until two conditions are satisfied: p_{new} reaches \mathbb{O} and $FRS(p_{\text{new}}, T_{\text{pred}})$ does not collide with the route of the ego vehicle. Fig. 3 shows the dynamic PVS obtained for a common intersection scenario. The dynamic PVS considers every potential dynamic PV that is *relevant* to the ego vehicle.

3) *Phantom Pedestrian Zone*: Unlike PVs, PPs can be anywhere. In [11], they called PPs outside a sidewalk or crosswalk, *illegally-behaving pedestrians*. Because the area of illegally-behaving pedestrians covers the area of legally-behaving pedestrians, we only considered illegally-behaving pedestrians. Given T_{pred} and route of the ego vehicle at time t_0 , the PPZ is defined as follows:

$$PPZ := \{p \in \mathbb{R}^2 \mid p = \mathbb{O}^c \cap BRS(x_k, T_{\text{pred}}), x_k \in \text{route}(x(t_0))\} \quad (7)$$

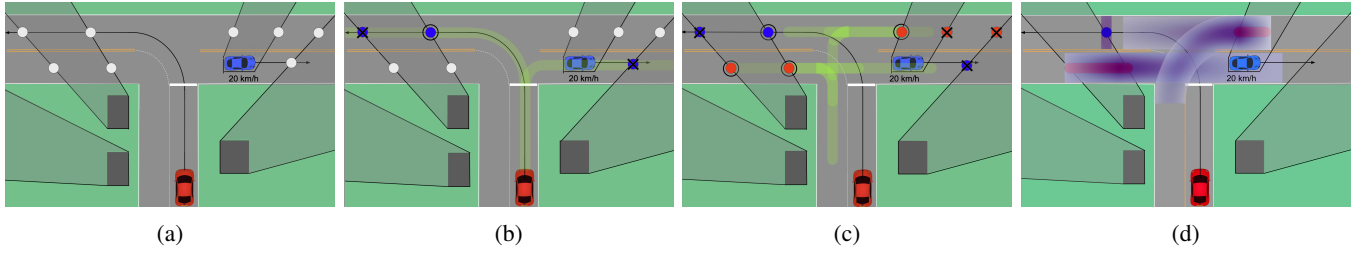


Fig. 2: Node classification: (a) application scenario where an ego vehicle (red) navigates an intersection having occluded areas (shaded in gray) and another vehicle (blue). Intersecting nodes are represented as white points. (b) Relevant static node (circled blue point) and irrelevant static nodes (crossed-out blue points) are classified according to the FRS of the dynamic nodes (shaded in yellow). (c) Relevant dynamic nodes (circled red points) and irrelevant dynamic nodes (crossed-out red points) are classified according to the FRS of the dynamic nodes (shaded in yellow). (d) Obtained phantom vehicle zone and its occlusion risk. The magenta carries the same meaning as in Fig. 1

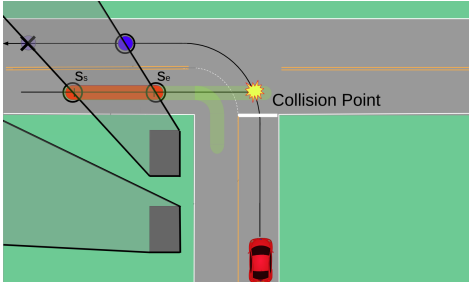


Fig. 3: Dynamic phantom vehicle set (PVS): The starting position of the dynamic PVS (red) is $(s_s, 0)$, and the end position is $(s_e, 0)$ where both positions are in the Frenet frame of PV. The forward reachable set (FRS) of the collision point is shaded in yellow.

Unlike the PVZ, no nodes are available for obtaining the FRS of PP. Therefore, we use the BRS of the route of the ego vehicle to find the PPZ. The furthest PP (i.e., the edge of the BRS of the PPs) from the route path of the ego vehicle along the shortest path. For a road such as that shown in Fig. 4, the PPZ can simply be obtained as the rectangular area along the route from which the observable polygon is subtracted.

C. Simplified Reachability Quantification

Strongly motivated by [4], [5], we improved upon their occlusion-aware risk assessment method by reducing the computational load. Our approach, namely SRQ, quantifies the reachability of dynamic PVS using a simple distribution model as follows.

SRQ quantifies the reachability of the dynamic PVS using the BRS with simple distribution model. Let T_{pred} be the prediction horizon in which it is impossible to avoid a collision with a suddenly appearing vehicle due to the computational time of the autonomous driving stack, the maximum velocity of PV v_{max} , the dynamic PVS, x be the initial position of a PV, y be the final position of a PV, and $g(y)$ amount of element of $BRS(y, T_{\text{pred}})$, which represents the amount of PVs that can reach y while satisfying below conditions. Here, PV is assumed to be driving along the lane. Therefore, x and y are defined as longitudinal positions in the Frenet frame of the PV, which can be anywhere within the dynamic PVS and can have random velocity. However, since no prior information is

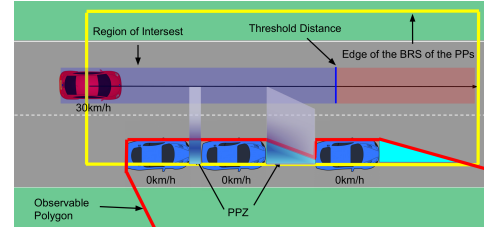


Fig. 4: Phantom pedestrian zone (PPZ): The ego vehicle (red) drives along other vehicles (blue) parked on the street. The PPZ (cyan) is derived from the BRS (yellow rectangle) of the route (black) and the observable polygon (red). The risk is represented as purple, and the darker the purple gets the riskier it is. The risk of PPs beyond a threshold distance (blue line) is filtered out.

provided, the initial position of PV is assumed to be uniformly distributed along the DPVS $[s_s, s_e]$ and the velocity of PV is constant and uniformly distributed $[0, v_{\text{max}}]$ like [5] did. The function $g(y)$ is defined in three intervals according to the value of y : $I_1 := [s_s, s_e]$, $I_2 := [s_e, s_s + v_{\text{max}}T_{\text{pred}}]$, and $I_3 := [s_s + v_{\text{max}}T_{\text{pred}}, s_e + v_{\text{max}}T_{\text{pred}}]$. Note that $s_e - s_s \leq v_{\text{max}}T_{\text{pred}}$ always satisfies by the definition of the dynamic PVS in Section IV-B.

Fig. 5 shows the BRS of PV depending on the value of y that satisfies the aforementioned assumptions, as gray-shaded polygon. Because the initial position and velocity of PV are assumed to be uniformly distributed, the area of gray-shaded polygon represents the PV that can reach y . Note that the conditions $x \in [s_s, s_e], v \in [0, v_{\text{max}}], t \in [0, T_{\text{pred}}]$ should be satisfied. The blue line represents the PV whose initial positions are already in y , therefore they reach y at $t = 0$ regardless of their velocities. The red line represents the PV that manages to reach y at $t = T_{\text{pred}}$. Because the velocity of PV is assumed to be constant, $y = x + vt$ is always satisfied. Using this condition, $g(y)$ is easily derived. For convenience, s is used instead of y because s is commonly used to represent the longitudinal position in the Frenet frame. This is graphed in Fig. 6 and is derived as follows:

$$g(s) := \begin{cases} \frac{1}{2}(2v_{\text{max}} - \frac{s-s_s}{T_{\text{pred}}})(s - s_s), & (s \in I_1) \\ \frac{1}{2}(2v_{\text{max}} - \frac{s-s_s}{T_{\text{pred}}} - \frac{s-s_e}{T_{\text{pred}}})(s_e - s_s), & (s \in I_2) \\ \frac{1}{2}(v_{\text{max}} - \frac{s-s_e}{T_{\text{pred}}})(s_e - (s - v_{\text{max}}T_{\text{pred}})), & (s \in I_3) \end{cases} \quad (8)$$

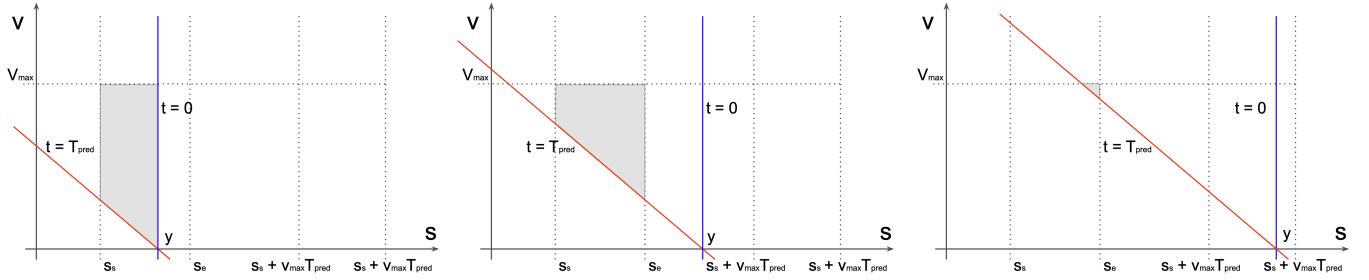


Fig. 5: The area of shaded in gray represents the $g(y)$. Each graph represents a different interval of $g(y)$ depending on the value of y .

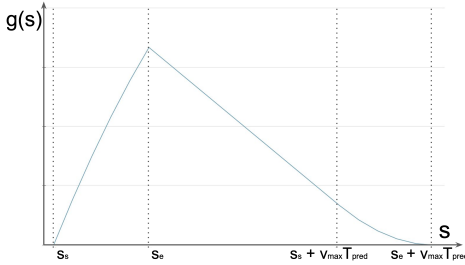


Fig. 6: SRQ along the longitudinal position in the Frenet frame of the dynamic PVS.

Here, (8) considers every possible motion of PV in every position of the dynamic PVS without prior information.

D. Risk Assessment

The PVZ and PPZ obtained from the previous steps is then applied to the risk assessment.

1) *Static Phantom Vehicle*: For the same reason why static PVS is defined to encompass relevant \mathbb{S} , PV in the static PVS is assumed to be stopped, which is an most efficient and safest approach to assess its risk.

2) *Dynamic Phantom Vehicles*: $g(s)$ from SRQ represents the amount of PV that can reach s . It can be interpreted as the occluded area (i.e., dynamic PVS) may contain a hidden vehicle with the ability to reach the position s , and the probability to reach position s increases as $g(s)$ increases. Therefore, $g(s)$ can be used to define an occlusion risk of dynamic PVS.

In Section IV-B, we assumed that an actual vehicle always exists in the dynamic PVS. The probability that an actual vehicle exists in the dynamic PVS should also be considered. Naturally, the probability increases if the dynamic PVS is longer. Therefore, the occlusion risk should be defined to be increased with a longer dynamic PVS. The occlusion risk $o(s)$ considering the probability of an actual vehicle existing in the dynamic PVS is defined as follows:

$$o(s) := (s_e - s_s) \cdot g(s) \quad (9)$$

However, assessing the risk of a dynamic PVS of which the collision point is too far from the ego vehicle is unnecessary. A more efficient approach is to filter out the dynamic PVS of which the collision point is farther than *static nodes* or a

threshold distance, which is proportional to the current velocity of the ego vehicle.

Because not every vehicle drives along the centerline of a road, the lateral deviation of PVs should be considered, which we assume can be represented as a normal distribution of which confidence interval of lateral deviation d (set to 90% for evaluation) is $[-l_w^k/2, l_w^k/2]$. Let $w(d) := N(0, (\frac{l_w^k}{2 \times Z(1-0.5(1-d))})^2)$. Then, the final distribution of the risk of the dynamic PVS can be defined as follows:

$$r(s, d) := o(s) \times w(d) \quad (10)$$

The occlusion risk that are on the route of the ego vehicle are illustrated in Fig. 2d.

3) *Phantom Pedestrians*: Unlike PVs, PPs can move in any direction. Thus, the FRS of a PP for a given T_{pred} can be assumed as a circle. However, PPs moving away from the route of the ego vehicle do not have to be considered, therefore the FRS can be assumed as a semicircle toward the route. Without prior information, PP could be assumed to move straight toward the closest point along the route. Since the expected heading angle of PP would be straightforward to the closest point along the route.

If the heading angle of the PP is fixed and with the same assumption used in risk assessment of PVs, the risk of PPs can be assessed in the same manner as for PV. Given $s_s, s_e, T_{\text{pred}}, v_{\text{max}}$, (9) can be used to assess the risk due to PPs. However, assessing the risk of PPs too far from the current position is unnecessary. Thus, such PPs should be filtered out as we did for unnecessary PVs as illustrated in Fig. 4.

E. Driving Strategy

There are lots of driving strategies when driving through an occluded area. One of them is to plan a trajectory that reduces the occlusion risk [4], [5], [9] or plan the velocity profile of a fixed path [7], [18]–[20]. The latter approach was chosen because expert drivers rarely change their path in common occluded scenarios such as intersections, roads with street parking, and narrow alleys. In addition, tuning the parameters for generating trajectories with and without occlusion risk would be difficult or would not work in the desired manner.

The occlusion risk obtained from SRQ can be used to control the velocity of the ego vehicle on a fixed path. The occlusion

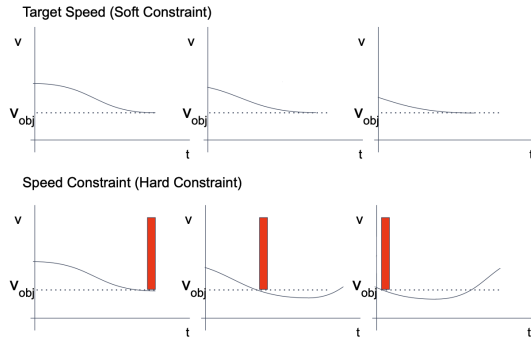


Fig. 7: Velocity planning delay. The same velocity is used as the target velocity and speed limit. The red square represents the speed limit due to occlusion risk.

risk can be used directly as a *cost function* for optimization or trajectory selection, lowering the *target velocity*, or adding a *speed limit* condition.

Using the occlusion risk as cost for optimization can yield a high computational load or even be infeasible because the occlusion risk distribution is spread over a large area. Lowering the target velocity is ineffective if the velocity is planned for every time step, which will delay the time taken by the ego vehicle to reach the target velocity as shown in Fig. 7 [21]. Adding a speed limit condition is an agile and effective approach that allows the ego vehicle to be aware of exact position where occlusion risk presents and guarantees that it slows down where expected. In addition, the speed limit is easily integrated with any planning algorithm by adding the extra constraint $v \leq v_{speed_limit}$ or selecting a trajectory that satisfies the speed limit among sampled trajectories.

1) *Speed Limit*: The speed limit $v_{speed_limit}^{occ}$ and its position p_{speed_limit} due to the occlusion risk are obtained as follows. First, the points along the route of the ego vehicle where an occlusion risk exists should be determined. Second, these points should be clustered. Third, the *weighted average* of the occlusion risk for these points should be obtained. Then, the speed limit and its position can be defined as follows:

$$p_{speed_limit}^{[c]} := \sum_{k=1}^{N^{[c]}} \frac{r_k^{[c]} \cdot p_k^{[c]}}{r_{total}^{[c]}} \quad (11)$$

where $c \in C$ is the cluster of points with an occlusion risk, $p_{speed_limit}^{[c]}$ is the weighted average position of occlusion risk for each cluster c , $N^{[c]}$ is number of points in cluster c , $p_k^{[c]}$ is the position of the point, $r_k^{[c]}$ is the occlusion risk of the point, and $r_{total}^{[c]}$ is the total sum of the occlusion risk defined in (10) for cluster c . Then,

$$v_{speed_limit}^{occ} = \begin{cases} \frac{v_{min}^{occ} - v_{max}^{occ}}{c_{min}^{th} - c_{max}^{th}} (r_{total}^{[c]} - c_{min}^{th}) + v_{max}^{occ}, & (c_{min}^{th} \leq r_{total}^{[c]} \leq c_{max}^{th}) \\ v_{min}^{occ}, & (c_{max}^{th} < r_{total}^{[c]}) \end{cases} \quad (12)$$

where c_{min}^{th} , c_{max}^{th} are the minimum and maximum occlusion risk threshold and v_{min}^{occ} , v_{max}^{occ} are the minimum and maximum



Fig. 8: The test vehicle. It is remodeled from a Hyundai Solati and equipped with several LIDAR, RADAR, and camera units.

speed limits when the occlusion risk is sufficient. $v_{speed_limit}^{occ}$ has a simple linear relation: it is low when the occlusion risk is high and vice versa. v_{min}^{occ} is for features of expert drivers who take risk and preventing the ego vehicle from freezing and never reaching the goal. If $c_{min}^{th} = 0$ and $v_{min}^{occ} = v_{max}^{occ} = 0$, then our proposed method obtains similar results as over-approximating methods.

2) *Planning*: Piecewise-jerk speed optimization (PJSO) method is chosen [22] for the velocity planning, which involves minimizing the cost function comprising the cost of ride discomfort (acceleration, jerk). The speed limit was added as a hard constraint to the optimization problem:

$$\dot{x}(t) < \min(\sqrt{a_{lateral_max}/\kappa(x)_{max}}, v_{speed_limit}^{occ}) \quad (13)$$

where $\kappa(x)_{max}$ is the maximum curvature of the ego vehicle and $a_{lateral_max}$ is maximum lateral acceleration along the fixed path. Together $\sqrt{a_{lateral_max}/\kappa(x)_{max}}$ represents the approximate speed limit due to the curvature of the fixed path.

V. EVALUATION

We compared our method with three *baseline* methods in various scenarios in the CARLA simulator and the real world with the test vehicle in Fig. 8. Fig. 9 shows the five scenarios implemented in CARLA. Furthermore, scenarios 1 and 5 were evaluated in the *real world*. In CARLA, each scenario was simulated 500 times with velocities randomly distributed in $[v_{speed_limit}^{road}, 1.5 \times v_{speed_limit}^{road}]$ and pedestrian with velocities randomly distributed in $[4\text{km/h}, 6\text{km/h}]$. Every method was implemented using the AMD Ryzen 7 series clocked at 2.2 GHz.

A. Baseline Methods

1) *Baseline 1*: *Baseline 1* used the *path velocity decomposition* method for trajectory planning without occlusion-aware risk assessment. The path is given by the route of the ego vehicle, and the velocity profile was generated using PJSO.

2) *Baseline 2*: *Baseline 2* was the same as *baseline 1* but with the SOTA occlusion-aware risk assessment algorithm proposed by [5]. Compare to *baseline 2*, our method was more robust in various scenarios and had better computational efficiency. However, the obtained occlusion risk for PVs was

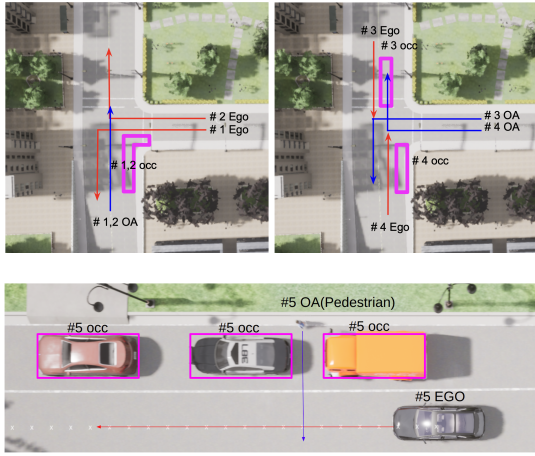


Fig. 9: Five scenarios in the CARLA simulator. Obstacles that induce occlusion are represented as magenta polygon. The ego vehicle drives along the route (red arrow) and counters occluded agent(OA) moving along its own route (blue arrow).

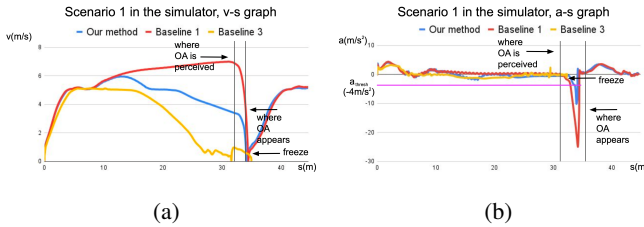


Fig. 10: Comparison between the proposed method (blue), baseline 1 (red), and baseline 3 (yellow) in the CARLA simulator (Scenario 1): The horizontal axis of graph (i.e., s) denotes the longitudinal position of the Frenet frame of the ego vehicle. $a_{th}(4m/s^2)$ is represented as magenta.

similar to our method, and [5] cannot be used in scenarios including occluded pedestrians. Thus, we could only compare the computational times of methods for scenarios without occluded pedestrians.

3) *Baseline 3*: *Baseline 3* also used the same planning method (i.e., baseline 1) but with another SOTA occlusion-aware risk assessment algorithm proposed by [3].

B. Metrics

We used five metrics to evaluate the methods: the discomfort score, collision rate, traversal time, freeze rate, and average computational time. The discomfort score from [5] was used to represent the discomfort of passengers in the ego vehicle and a_{th} was chosen as $4m/s^2$:

$$\text{Discomfort Score} = \frac{1}{T} \int_0^T \max(0, |a_{ego}(t)| - a_{th}) dt$$

The freeze is defined as a situation when the ego vehicle doesn't go any further because the occlusion risk presented in front of the ego vehicle prevents the ego vehicle from moving forward.

VI. RESULT

Compared with baseline 1, our proposed method decreased the collision rate and the discomfort score by up to 6.14 times

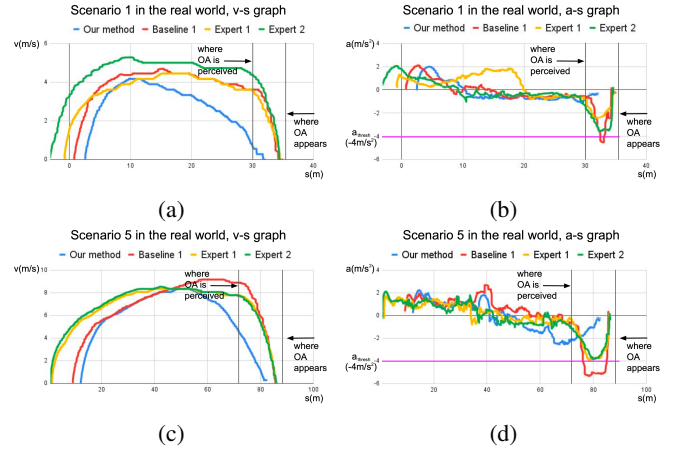


Fig. 11: Comparison between the proposed method (blue), baseline 1 (red), and expert drivers (yellow and green) in the real world (Scenario 1, 5): The horizontal axis of graph (i.e., s) denotes the longitudinal position of the Frenet frame of the ego vehicle. $a_{th}(4m/s^2)$ is represented as magenta.

and 5.03 times, respectively, while it increased the traversal time by 1.48 times. In addition, our method decreased traversal time by up to 1.58 times, while it increased the collision rate by 0.4%, compared to baseline 3. In Table.I, baseline 1 showed the shortest traversal time, while resulting in the highest collision rate and discomfort score. This is because baseline 1 doesn't consider the sudden appearance of OAs. On the other hand, baseline 3 was overcautious about OAs, resulting in the longest traversal time or even freeze in heavily occluded scenarios, while having the lowest collision rate and discomfort score. However, the proposed method efficiently assessed occlusion risk, resulting in a small increase in collision rate and discomfort score while decreasing considerable traversal time. The proposed method performed better in scenarios 3 and 4 than in scenarios 1 and 2. This is because the routes of the ego vehicle in scenarios 1 and 2 included left/right turns, which made the ego vehicle slow down before reaching the speed limit due to occlusion. Therefore, the differences between the velocity profiles with our method and with baseline 1 were unclear.

Fig. 10 compared the proposed method, baseline 1, and baseline 3 for scenario 1 in the CARLA simulator and Fig. 11 compared the proposed method, baseline 1, and expert drivers for scenarios 1 and 5 in the real world. In Fig.10, every method managed to safely stop and avoid collision with a suddenly appearing agent. However, our method reduced the velocity before entering the intersection which prevented sudden deceleration and collision while baseline 1 didn't reduce the velocity and ended up with sudden deceleration. In addition, baseline 3 was overcautious about OAs and reduced the velocity more than our method before entering the intersection. At the intersection, baseline 3 froze because of its conservativeness. In Fig.11, expert drivers showed safe and comfort driving without losing efficiency. Our method reduced the velocity earlier than expert drivers, which made the driving much comfortable but lost some efficiency. This trade-off between driving comfort and efficiency is inevitable. Our method can adjust the magnitude of the trade-off by tuning

TABLE I: Performance Comparison Between the Proposed Method, Baseline 1, and Baseline 3 in the CARLA simulator

Scenario	Collision rate	Discomfort score	Traversal time	Freeze rate
1 Proposed	6.00%	0.0251	20.63s	0.00%
Baseline 1	15.80%	0.0663	14.22s	0.00%
Baseline 3	0.00%	0.0237	31.54s	70.00%
2 Proposed	0.20%	0.0008	16.82s	0.00%
Baseline 1	0.60%	0.0009	15.00s	0.00%
Baseline 3	0.00%	0.0008	27.31s	0.60%
3 Proposed	1.40%	0.0009	12.97s	0.00%
Baseline 1	8.60%	0.0047	8.75s	0.00%
Baseline 3	0.00%	0.0008	21.63s	0.00%
4 Proposed	0.40%	0.0004	17.4s	0.00%
Baseline 1	1.20%	0.0020	11.1s	0.00%
Baseline 3	0.00%	0.0003	27.6s	0.00%
5 Proposed	10.00%	0.0065	13.78s	0.00%
Baseline 1	24.00%	0.0186	12.58s	0.00%
Baseline 3	0%	0.0012	30.3s	97.80%

TABLE II: Average Computational Times of the Proposed Method, Baseline 2, and Baseline 3 in the CARLA simulator.

Computation Time Table				
Scenario #	1	2	3	4
Proposed	1.3029ms	1.5005ms	1.6467ms	2.6913ms
Baseline 2	26.2528ms	18.6865ms	32.0241ms	39.9024ms
Baseline 3	1.2693ms	1.3453ms	1.4322ms	2.3604ms

the parameters such as threshold distance and v_{\min}^{occ} . A video of the experiments is available at <https://youtu.be/TJo2pfhkxw4>.

Table II compares the average computational times of *baseline 2*, *3*, and our method. Even though we set *baseline 2* to $N_k \leq 4 \cdot 10^4$, which is a much smaller number of particles than used by [5], our method reduced computational time by up to 20.15 times. Moreover, our method quantified the risk of PAs while having a similar computational efficiency to baseline 3.

VII. CONCLUSIONS AND FUTURE WORK

We proposed the occlusion-aware risk assessment method and planning strategy using SRQ that improves upon the work of other authors [3]–[5], [10] by extending the risk assessment to occluded pedestrians and reducing the computational load. We evaluated our method in various scenarios and the results showed that our method effectively decreased the collision rate and discomfort score while greatly reducing the computational time compared with the current state-of-the-art methods. Future work will involve using sequential reasoning to remove redundant PAs and improve the driving efficiency of the ego vehicle by preventing conservative behavior.

REFERENCES

- [1] Pongsathorn Raksincharoensak, Takahiro Hasegawa, and Masao Nagai. Motion planning and control of autonomous driving intelligence system based on risk potential optimization framework. *International Journal of Automotive Engineering*, 7(AVEC14):53–60, 2016.
- [2] Shane Gilroy, Edward Jones, and Martin Glavin. Overcoming occlusion in the automotive environment—a review. *IEEE Transactions on Intelligent Transportation Systems*, 22(1):23–35, 2019.
- [3] Markus Koschi and Matthias Althoff. Set-based prediction of traffic participants considering occlusions and traffic rules. *IEEE Transactions on Intelligent Vehicles*, 6(2):249–265, 2020.
- [4] Ming-Yuan Yu, Ram Vasudevan, and Matthew Johnson-Roberson. Risk assessment and planning with bidirectional reachability for autonomous driving. In *2020 IEEE International Conference on Robotics and Automation (ICRA)*, pages 5363–5369. IEEE, 2020.
- [5] Ming-Yuan Yu, Ram Vasudevan, and Matthew Johnson-Roberson. Occlusion-aware risk assessment for autonomous driving in urban environments. *IEEE Robotics and Automation Letters*, 4(2):2235–2241, 2019.
- [6] Alexey Dosovitskiy, German Ros, Felipe Codevilla, Antonio Lopez, and Vladlen Koltun. Carla: An open urban driving simulator. In *Conference on robot learning*, pages 1–16. PMLR, 2017.
- [7] Stephen G McGill, Guy Rosman, Teddy Ort, Alyssa Pierson, Igor Gilitschenski, Brandon Araki, Luke Fletcher, Sertac Karaman, Daniela Rus, and John J Leonard. Probabilistic risk metrics for navigating occluded intersections. *IEEE Robotics and Automation Letters*, 4(4):4322–4329, 2019.
- [8] Minchul Lee, Kichun Jo, and Myoungcho Sunwoo. Collision risk assessment for possible collision vehicle in occluded area based on precise map. In *2017 IEEE 20th International Conference on Intelligent Transportation Systems (ITSC)*, pages 1–6. IEEE, 2017.
- [9] Lingguang Wang, Carlos Fetnandez Lopez, and Christoph Stiller. Generating efficient behaviour with predictive visibility risk for scenarios with occlusions. In *2020 IEEE 23rd International Conference on Intelligent Transportation Systems (ITSC)*, pages 1–7. IEEE, 2020.
- [10] Piotr F Orzechowski, Annika Meyer, and Martin Lauer. Tackling occlusions & limited sensor range with set-based safety verification. In *2018 21st International Conference on Intelligent Transportation Systems (ITSC)*, pages 1729–1736. IEEE, 2018.
- [11] Yannik Nager, Andrea Censi, and Emilio Frazzoli. What lies in the shadows? safe and computation-aware motion planning for autonomous vehicles using intent-aware dynamic shadow regions. In *2019 International Conference on Robotics and Automation (ICRA)*, pages 5800–5806. IEEE, 2019.
- [12] José Manuel Gaspar Sánchez, Truls Nyberg, Christian Pek, Jana Tumova, and Martin Törngren. Foresee the unseen: Sequential reasoning about hidden obstacles for safe driving. In *2022 IEEE Intelligent Vehicles Symposium (IV)*, pages 255–264. IEEE, 2022.
- [13] Kristijan Macek, Dizan Alejandro Vasquez Govea, Thierry Fraichard, et al. Towards safe vehicle navigation in dynamic urban scenarios. *Automatika—Journal for Control, Measurement, Electronics, Computing and Communications*, 2009.
- [14] Sara Bouraine, Thierry Fraichard, and Hassen Salhi. Provably safe navigation for mobile robots with limited field-of-views in dynamic environments. *Autonomous Robots*, 32:267–283, 2012.
- [15] Shai Shalev-Shwartz, Shaked Shammah, and Amnon Shashua. On a formal model of safe and scalable self-driving cars. *arXiv preprint arXiv:1708.06374*, 2017.
- [16] Christian Pek and Matthias Althoff. Computationally efficient fail-safe trajectory planning for self-driving vehicles using convex optimization. In *2018 21st International Conference on Intelligent Transportation Systems (ITSC)*, pages 1447–1454. IEEE, 2018.
- [17] Matthias Althoff and Silvia Magdici. Set-based prediction of traffic participants on arbitrary road networks. *IEEE Transactions on Intelligent Vehicles*, 1(2):187–202, 2016.
- [18] M Sadou, V Polotski, and P Cohen. Occlusions in obstacle detection for safe navigation. In *IEEE Intelligent Vehicles Symposium, 2004*, pages 716–721. IEEE, 2004.
- [19] Maximilian Naumann, Hendrik Konigshof, Martin Lauer, and Christoph Stiller. Safe but not overcautious motion planning under occlusions and limited sensor range. In *2019 IEEE Intelligent Vehicles Symposium (IV)*, pages 140–145. IEEE, 2019.
- [20] Maxime Bouton, Alireza Nakhaei, Kikuo Fujimura, and Mykel J Kochenderfer. Scalable decision making with sensor occlusions for autonomous driving. In *2018 IEEE international conference on robotics and automation (ICRA)*, pages 2076–2081. IEEE, 2018.
- [21] Moritz Werling, Julius Ziegler, Sören Kammel, and Sebastian Thrun. Optimal trajectory generation for dynamic street scenarios in a frenet frame. In *2010 IEEE International Conference on Robotics and Automation*, pages 987–993. IEEE, 2010.
- [22] Jinyun Zhou, Runxin He, Yu Wang, Shu Jiang, Zhenguang Zhu, Jiangtao Hu, Jinghao Miao, and Qi Luo. Autonomous driving trajectory optimization with dual-loop iterative anchoring path smoothing and piecewise-jerk speed optimization. *IEEE Robotics and Automation Letters*, 6(2):439–446, 2020.